# Loss-spectroscopy on sparse arrays of aligned carbon nanotubes

**Christian Kramberger[*,1,2], Mark Rümmeli[1] Martin Knupfer[1], Jörg Fink[1,3], Bernd Büchner[1], Erik Einarsson[4], Shigeo Maruyama[4], and Thomas Pichler[1,2]**

[1] IFW Dresden, Helmholtzstraße 20, D-01069 Dresden, Germany
[2] University of Vienna,Faculty of Physics, Strudlhofgasse 4, A-1090, Vienna, Austria
[3] BESSY, Albert-Einstein-Strae 15, D-12481 Berlin, Germany
[4] University of Tokyo, Department of Mechanical Engineering, 7-3-1 Hongo, Bunkyo-ku, Tokyo 113-8656, Japan

Received 23 April 2008, revised XXXX, accepted XXXX
Published online XXXX

**PACS** 73.20.Mf, 73.22.-f, 78.20.Bh

[*] Corresponding author: e-mail C.Kramberger@ifw-dresden.de, Phone: +49 351 4659 641, Fax: +49 351 4659 444, Web: www.ifw-dresden.de

We performed angle resolved electron energy-loss spectroscopy on vertically aligned single wall carbon nanotubes. We observe two distinct loss-peaks in the energy range from $4.6\,eV$ to $5.1\,eV$. This duplet of loss-peaks is attributed to the collective on-axis and crossed plasma oscillations of the $\pi$ electrons in $sp^2$ carbon. The unique identification and assignment of these two orientations is derived from their dispersion relations. The available momenta are aligned on the nanotube axis and reflect the confinement of a particle on a wire. The observed angle resolved loss-peaks are a gapless extension of polarized optical spectroscopy into finite momenta.



**1 Introduction** Single-wall carbon nanotubes (SWNT) are archetypes of low dimensional systems with strongly anisotropic and unique electronic properties, which make them interesting for fundamental research and as building blocks in nanoelectronic applications [1,2]. SWNT exhibit two distinct ultra violet absorption peaks for on-axis and crossed polarization in optical absorption spectroscopy (OAS). In bulk samples the on-axis polarized peak is at $\sim 4.5\,eV$ [3] and in vertically aligned SWNT (VA-SWNT) an additional cross-polarized peak is observed at $\sim 5.2\,eV$ [4]. The full electronic excitation spectrum beyond the optical limit of vanishing momentum for all itinerant, namely the $\pi$ and the $\sigma$ electrons, is accessible by electron energy loss-spectroscopy (EELS) [5]. Angle resolved EELS (AR-EELS) assesses the detailed plasmon dispersion [6,7,8] and retrieves fundamental information on the available momentum space, viz. structural confinement.

The present work addresses AR-EELS studies on the momentum $(\mathbf{q})$ dependent electronic excitations of vertically aligned SWNT (VA-SWNT). The one to one match of the optical limit $q \to 0$ of the $\pi$ plasmon dispersions to the $\pi$ peak positions in polarized OAS is fully described within the feasible Drude-Lorentz model. The distinct on-axis as well as crossed dispersions $\omega(\mathbf{q})$ of the $\pi$ plasmon energies expose a localized crossed as well as a propagating on-axis signature.

**2 Methods** Forests of VA-SWNT were directly grown from a binary CoMo catalyst on quartz substrates and alcohol vapor. The film thickness was monitored in situ via optical absorption. The current batch comprises $2\,\mu m$ to $7\,\mu m$ thick films. The as prepared films were floated off in hot water and recaptured onto Cu grids [9]. The nematic order as well as optical properties [4,10] and local morphology [11] of the VA-SWNT have been studied earlier. The VA-SWNT are aligned within $25^\circ$ and typically packed in thin bundles with less than 10 nanotubes. The diameter of the individual tubes is typically $\sim 2\,nm$. The angle resolved loss function of the VA-SWNT was measured in a purpose built EELS spectrometer [12]. The primary probe beam of high-energy electrons traverses the freestanding VA-SWNT perpendicularly and the inelastic scattering events are registered. Earlier comparative EELS studies were performed on a cleaved single crystal of

graphite [13] or bundled and magnetically aligned SWNT (MA-SWNT) [14, 7]. In the present study we set an energy and momentum resolution of $200\,meV$ and $0.05\,\mathring{A}^{-1}$.

**3 Results & Discussion** Figure 1 shows a compilation of transmission electron microscopy (TEM) micrographs of the freely suspended VA-SWNT material.Typically the film does not entirely span the open hexagons of the Cu grid, but leaves an open area in the center. Zooming in on the light gray film from Fig. 1a reveals a rather inhomogeneous internal structure in Figs. 1b&1c. Most of the films internal space is just empty and the entire density is typically concentrated in the nanometer large dark dots. An even closer look in Fig. 1d reveals that all of these dark dots are actually bundles of a few SWNT that are quite frequently passing the focal plane of the micrograph. A quantitative statistical evaluation of bundle sizes can be found in Ref. [11]. The local morphological investigations do further suggest a really low macroscopic density as well as a fairly poor percolation. From the optical absorbance and film height the density of VA-SWNT material has been estimated to be roughly $\rho_V \sim 3 \cdot 10^3\, mol/m^3$. The latter corresponds to $\rho_V \sim 0.04\, g/cm^3$. Hence, the bulk density of VA-SWNT is less than 2% of the bulk density of graphite $\rho_G \sim 2.3\, g/cm^3$.

The wide open channels, facing the electron beam, and the remarkable low density of the VA-SWNT films account for the clear electron transparency of the $\mu m$ thick films. The excellent electron transparency not only enables TEM imaging but also prepares the ground for AR-EELS. Inelastic electron scattering probes the electronic loss-function which is connected to the complex dielectric function via $I \propto \mathrm{Im}(\varepsilon^{-1})$ [15]. The most feasible description of the dielectric function comes in the framework of the classical Drude Lorentz model. Therein the longitudinal plasma frequencies $\omega_{\mathrm{L}}$ of the loss-peaks are with respect to the transversal optical absorption peaks $\omega_{\mathrm{T}}$ upshifted by the plasma frequency $\omega_{\mathrm{P}}^2 = (n \cdot e^2)/(m^\star \cdot \varepsilon_0)$ according to $\omega_{\mathrm{L}}^2 = \omega_{\mathrm{T}}^2 + \omega_{\mathrm{P}}^2$. As a consequence of the latter statement loss-peaks are always measured at higher energies than the corresponding absorption peaks. While this upshift is always present in regular bulk material, it can vanish for quasi isolated nano-objects with a low bulk density. Archetypical examples of dielectric function and the related spectral functions of these two cases are provided in Fig. 2.

Indeed, the fairly different densities of bulk graphite and the sparsely arranged VA-SWNT are reflected in very different plasmon energies for the $\pi$ and the more structured $\pi + \sigma$ plasmons. The loss-functions of graphite and VA-SWNT at a momentum transfer $q = 0.1\mathring{A}^{-1}$ are given in Fig. 3. We observe the $\pi$ plasmons of bulk graphite and sparse VA-SWNT at $\sim 6.9\,eV$ and $\sim 5.1\,eV$, respectively. The broader and more structured $\pi + \sigma$ shows an even bigger shift from $\sim 27.3\,eV$ to $\sim 17.6\,eV$.

The noticeable shift in the plasmon frequencies is not only an independent confirmation of the low density by a bulk sensitive method, but it also motivates further momentum resolved studies at larger momentum transfers $q$. The loss-function at different fixed momentum transfers $q$ (viz. scattering geometries) is exposed in Fig. 4. The following discussion will be focused on the (more clear) observations on the $\pi$ region, but we still want to point out that the same arguments also apply to the $\pi + \sigma$ region. Consistently, all collective electronic excitations share the same universal behavior. The loss-function at high momentum reveal a twofold plasmon dispersion. The individual dispersions of the two independent $\pi$ plasmons are traced by dashed arrows. Apparently there is fundamental distinction between a dispersive and a non-dispersive plasmon response. The individual behaviors are well known, either as dispersive plasmons that are propagating in solids or as non-dispersive plasmons that are confined on a molecule [16]. The intriguing aspect is that these two fundamentally different behaviors are observed simultaneously in the very same loss-functions. The direct conclusion is that the VA-SWNT inherently bear properties of molecules *and* solids

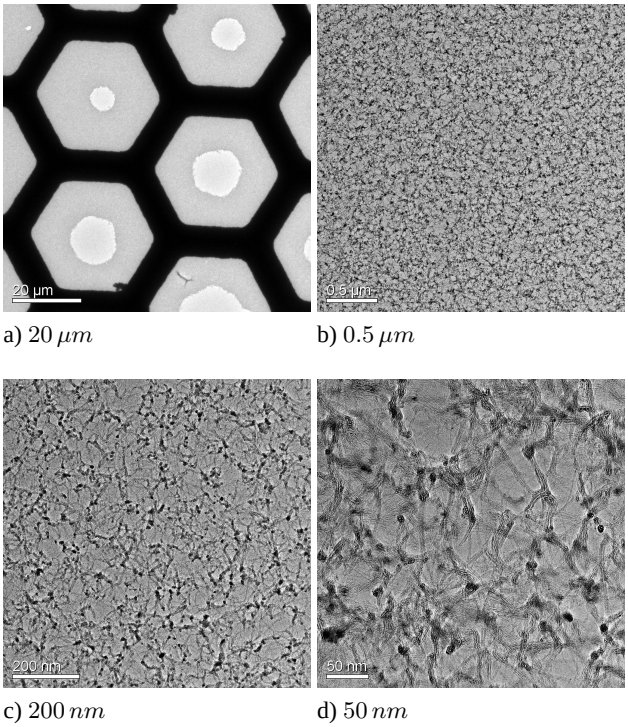


a) $20\,\mu m$ b) $0.5\,\mu m$

c) $200\,nm$ d) $50\,nm$

**Figure 1** TEM micrographs of freestanding films of VA-SWNT. The macroscopic shape is a holey film on the TEM grid. The local morphology consists of thin bundles of a few ($< 10$) individual SWNT. The bundles are preferably oriented perpendicular to the imaging plane. The length of the individual scale bars is given underneath the respective micrographs.

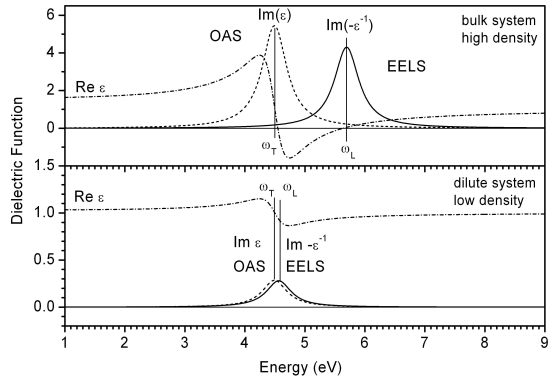


**Figure 2** Characteristic features of the dielectric function of a single electronic Lorentz oscillator $\varepsilon(\omega) = \varepsilon_\infty + \omega_P^2/(\omega_T^2 - \omega^2 - i\omega\gamma)$ with $\varepsilon_\infty = 1$ an oscillator frequency $\hbar \cdot \omega_T = 4.5\ eV$ and a damping $\hbar \cdot \gamma = 0.5\ eV$. In the upper panel the oscillator strength is typical for bulk systems $\hbar \cdot \omega_P = 3.5\ eV$ and in the lower panel the oscillator strength is lowered to illustrate the coincidence of loss- and absorbtion spectroscopy in isolated objects $\hbar \cdot \omega_P = 0.8\ eV$. In either one case the real part of $\varepsilon$ is dash-dotted, the imaginary is plotted dashed and the loss-function is the solid line.

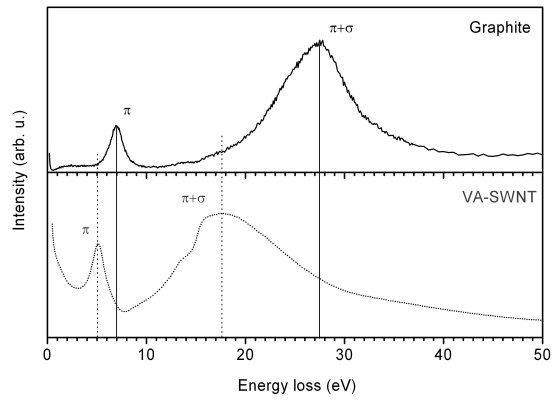


**Figure 3** The loss-function $I \propto \mathrm{Im}(\varepsilon^{-1})$ as probed by AR-EELS on bulk graphite (solid line) and sparse arrays of aligned nanotubes (dotted line) at a finite momentum transfer $q = 0.1\,\mathring{A}^{-1}$. The positions of the respective $\pi$ and $\pi + \sigma$ plasmons are marked by vertical lines.

at the same time. The tubular symmetry splits the collective $\pi$ plasmon in two, a propagating mode with $\mathbf{q}$ parallel to the nanotubes axis and a fully localized crossed mode. The first mode disperses with $\mathbf{q}$ along the nanotubes axis and the latter does not show any dispersion. The thin bundles of VA-SWNT are well separated from one another and appear as one-dimensional quantum wires to the collective plasmon modes.

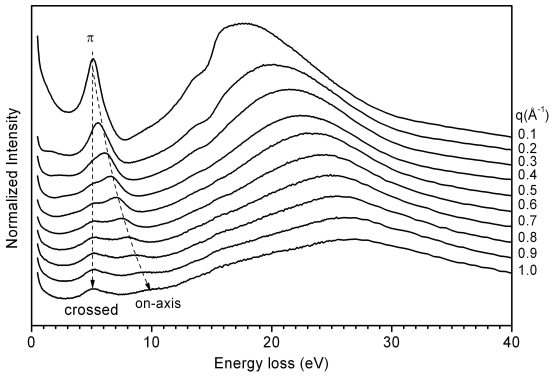


**Figure 4** Angle resolved loss-functions of VA-SWNT at various momentum transfers $0.1\,\mathring{A}^{-1} \leq q \leq 1.0\,\mathring{A}^{-1}$. The dispersions of the two $\pi$ plasmons are traced by dotted guides to the eye.

The plasmon frequency $\omega_\mathrm{L}$ in the optical limit $q \to 0$ is not directly accessible in the experiment due the proximity to the direct electron beam. Still experiments at finite $q$ allow one to identify the shape of the dispersion and enable tracing the experimental plasmon frequencies back onto their origin at $q = 0$. The dispersion of the two $\pi$ plasmons are presented in Fig. 5. At small momentum transfers only one peak is resolvable and only the dispersion of the joint peak can be evaluated. These joint positions comprise both underlying individual plasmon dispersions in an indiscernible way. The non-dispersive plasmon is found to be fully localized, there is no observable bandwidth up to $2.5\,\mathring{A}^{-1}$. The dispersive $\pi$ plasmon is found to be strictly linear. In the optical limit the dispersive on-axis $\pi$ plasmon would be at $\sim 4.6\,eV$ and the crossed $\pi$ plasmon would be at $\sim 5.1\,eV$. These values meet the two peak positions that are found by OAS for parallel polarizations along the SWNT axis or perpendicular polarization crossing the SWNT axis, respectively. Murakami *et al.* [4] identified the on-axis and cross polarized absorption peaks of the electronic $\pi$ system at $4.5\,eV$ and $5.25\,eV$. Hence, either spectroscopic method, namely AR-EELS and polarized OAS, provide their own self contained identification of the on-axis and the crossed response. The independent cross-confirmation of the identification of the on-axis and crossed excitations in isolated nanotubes is a firm experimental finding. The actual absorption features do even quantitatively reproduce the optical limit of the plasmon dispersions. This is only possible if the upshift due to lower plasma frequency $\omega_\mathrm{P}$ is negligible in VA-SWNT. Indeed the low density as well as the morphology of isolated quantum wires in the VA-SWNT account for both

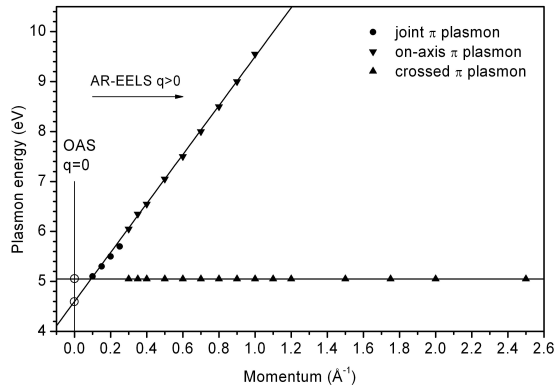


**Figure 5** Dispersion of the $\pi$ plasmons in VA-SWNT. At small $q < 0.3\,\mathring{A}^{-1}$ only the mean position of the crossed and the on-axis $\pi$ plasmon are given. The linear extrapolation to the optical limit $q = 0$ is marked by open circles.

the symmetry breaking into on-axis and crossed collective charge excitations as well as the quantitative correspondence of AR-EELS and OAS. Another interesting observation is the crossing of the split plasmon bands at finite momenta $\sim 0.1\,\mathring{A}^{-1}$ and the simultaneous signature of one-dimensional confinement in the loss-functions. In a truly one-dimensional system two (one- dimensional) plasmon bands could never cross one another. Apparently neither the full tubular structure nor crossed plasmon modes could be described by only one single space coordinate. The VA-SWNT are three dimensional isolated nano-objects, and due to one-dimensional confinement they act as quantum wires to their collective electronic excitations. We conclude, that the on-axis plasmons in the collective excitation spectrum of nanotubes are indeed one-dimensional quasi-particles.

**4 Summary** AR-EELS uncovers a symmetry breaking of the two-dimensional in-plane $\pi$ as well as $\pi + \sigma$ plasmons into propagating on-axis plasma excitations and crossed fully localized modes. Due to the negligible averaged density of isolated nanotubes the plasmon dispersions from AR-EELS are a gapless continuation of the full electronic excitation spectrum far beyond its optical $q \to 0$. Sparse arrays of isolated carbon nanotubes archetypes expose one-dimensional confinement in the electronic excitation spectrum to bulk sensitive spectroscopic methods. In analogy to the famous ‘particle in a box’, the confined on-axis plasmons are a prime example of ‘particles on a wire’.

**Acknowledgements** This work was supported by the DFG PI 440 4. C. K. acknowledges the *IMPRS for Dynamical Processes in Atoms, Molecules and Solids*. We thank S. Leger, R. Hübel, and R. Schönfelder for technical assistance.



## References

[1] P. Avouris and J. Chen, Mat. Today **9**(10), 46–54 (2006).
[2] J. C. Charlier, X. Blase, and S. Roche, Rev. of Mod. Phys. **79**(2), 677 (2007).
[3] H. Kataura, Y. Kumazawa, Y. Maniwa, I. Umezu, S. Suzuki, Y. Ohtsuka, and Y. Achiba, Synth. Met. **103**(1-3), 2555–2558 (1999).
[4] Y. Murakami, E. Einarsson, T. Edamura, and S. Maruyama, Phys. Rev. Lett. **94**(8), 087402 (2005).
[5] O. Stephan, D. Taverna, M. Kociak, K. Suenaga, L. Henrard, and C. Colliex, Phys. Rev. B **66**(15), 155422 (2002).
[6] T. Pichler, M. Knupfer, M. S. Golden, J. Fink, A. Rinzler, and R. E. Smalley, Phys. Rev. Lett. **80**(21), 4729–4732 (1998).
[7] X. Liu, T. Pichler, M. Knupfer, M. S. Golden, J. Fink, D. A. Walters, M. J. Casavant, J. Schmidt, and R. E. Smalley, Synth. Met. **121**(1-3), 1183–1186 (2001).
[8] C. Kramberger, R. Hambach, C. Giorgetti, M. Rummeli, M. Knupfer, J. Fink, B. Buchner, L. Reining, E. Einarsson, S. Maruyama, F. Sottile, K. Hannewald, V. Olevano, A. Marinopoulos, and T. Pichler, Phys. Rev. Lett. **in print** (2008).
[9] Y. Murakami and S. Maruyama, Chem. Phys. Lett. **422**(4-6), 575–580 (2006).
[10] C. Kramberger, H. Shiozawa, H. Rauf, A. Gruneis, M. H. Rummeli, T. Pichler, B. Buchner, D. Batchelor, E. Einarsson, and S. Maruyama, Phys. Stat. Solidi B **244**, 3978 (2007).
[11] E. Einarsson, H. Shiozawa, C. Kramberger, M. H. Rummeli, A. Gruneis, T. Pichler, and S. Maruyama, J. Phys. Chem. C **111**(48), 17861–17864 (2007).
[12] J. Fink, Adv. Elec. & Elec. Phys. **75**, 121–232 (1989).
[13] A. G. Marinopoulos, L. Reining, V. Olevano, A. Rubio, T. Pichler, X. Liu, M. Knupfer, and J. Fink, Phys. Rev. Lett. **89**(7), 076402 (2002).
[14] D. A. Walters, M. J. Casavant, X. C. Qin, C. B. Huffman, P. J. Boul, L. M. Ericson, E. H. Haroz, M. J. O’Connell, K. Smith, D. T. Colbert, and R. E. Smalley, Chem. Phys. Lett. **338**(1), 14–20 (2001).
[15] L. van Hove, Phys. Rev. **95**, 249 (1954).
[16] M. Knupfer, T. Pichler, M. S. Golden, J. Fink, A. Rinzler, and R. E. Smalley, Carbon **37**(5), 733–738 (1999).